Research Square

Preprints are preliminary reports that have not undergone peer review.
They should not be considered conclusive, used to inform clinical practice,
or referenced by the media as validated information.

Marine volatile organic compound exchange reorganizes compositionally on event-to-season timescales

Mehrshad Foroughan

mehrshad.foroughan@bio.ku.dk

University of Copenhagen https://orcid.org/0000-0001-8814-5420

Thomas Holst

Lund University

Kaisa Kraft

Finnish Environment Institute

Martti Honkanen

Finnish Meteorological Institute

Lauri Laakso

Finnish Meteorological Institute

Heidi Hellen

Finnish Meteorological Institute https://orcid.org/0000-0001-7022-3857

Jukka Seppälä

Finnish Meteorological Institute

Ken Stenbäck

Finnish Meteorological Institute

Christa Marandino

Leibniz Inst Meereswissensch

Riikka Rinnan

University of Copenhagen https://orcid.org/0000-0001-7222-700X

Physical Sciences - Article

Keywords:

Posted Date: March 13th, 2026

DOI: https://doi.org/10.21203/rs.3.rs-8785827/v1

License: This work is licensed under a Creative Commons Attribution 4.0 International License.
Read Full License

Additional Declarations: The authors declare no competing interests.

Version of Record: A version of this preprint was published at Nature Communications on November 23rd, 2026. See the published version at https://doi.org/10.1038/s41467-026-79437-1.

Abstract

Marine ecosystems influence atmospheric chemistry and climate by exchanging volatile organic compounds (VOCs) with the atmosphere, yet the chemical diversity and the environmental controls of the exchanged compounds remain poorly constrained at ecosystem timescales. This gap persists because most marine observations are targeted, short-term, and narrow-suite measurements that seldom deliver chemically broad, continuous fluxes. Here we show that marine VOC exchange is chemically diverse and changes in magnitude and composition on event-to-season timescales. Using continuous flux measurements of 48 compounds in the Baltic Sea, we observe a pronounced reorganization of net exchange: early organosulfur emissions diminish as cyanobacterial biomass declines (indicating water-side source limitation), while oxygenated and nitrogen-containing VOCs exhibit mixed behaviors ranging from deposition to episodic emissions (often driven by kinetic factors). Together, these results demonstrate that chemically diverse marine VOC exchange is closely coupled to wind-induced mixing, water-column structure, and phytoplankton community succession, highlighting the need to resolve these dynamic ecosystem states to predict future atmospheric composition.

Main

Non-methane volatile organic compounds (VOCs) are short-lived climate forcers that shape atmospheric oxidant budgets, tropospheric ozone, and secondary organic aerosol, with significant near-term impacts on air quality and radiative forcing[5]. In marine settings, VOC observations have focused on individual compounds, most notably DMS[6–8], isoprene[9,10], and selected oxygenated VOC, such as methanol[11,12], acetone[13,14], and acetaldehyde[15,16], using targeted approaches that limit chemical breadth and simultaneous flux inference. Although the measured suite is expanding (e.g., methanethiol[7,17]), continuous, chemically broad flux observations over the ocean remain scarce. Marine VOC emissions may rival or exceed terrestrial sources for key compounds like organosulfurs[18] and certain oxygenated VOCs[19], yet their global budget contributions are highly uncertain due to sparse observations and limited chemical coverage. By contrast, over land, eddy-covariance studies using Proton-Transfer-Reaction Time-of-Flight Mass Spectrometry (PTR-TOF-MS) demonstrated over a decade ago[20] that real-time, multi-compound measurements can capture ecosystem-scale exchange of many VOCs. The narrow scope of marine deployments risks overlooking climate-relevant compounds and masks VOC diversity across the ocean's vast surface.

A concurrent challenge remains in resolving temporal dynamics: seasonal and episodic changes in mixing and plankton community structure likely alter VOC composition and exchange. While ship transects capture spatial gradients[12,21,22] they struggle to resolve temporal variability. Here, we assess marine VOC exchange diversity using continuous observations at a fixed station, linking flux variability to physical and biological drivers within a consistent footprint. We conducted measurements at Utö Island in the Baltic Sea (Fig. 1), coupling PTR-TOF-MS with eddy covariance to measure VOC mixing ratios and direct air-sea fluxes, alongside meteorological, hydrographic, and phytoplankton observations. The

53-day campaign (summer–autumn 2024) captured the transition from stratified, productive conditions to cooler, mixed waters. This integrated approach provided the continuity and chemical breadth needed to attribute VOC fluxes to evolving wind, water-column structure, and phytoplankton composition.

Chemical diversity and temporal patterns of marine atmospheric VOCs

We detected >200 m/z features corresponding to potential VOCs in the marine atmosphere. After quality control (Methods), 48 VOC masses with confident chemical assignments remained, far exceeding the limited compounds measured in prior targeted campaigns[15,21,23]. We used redundancy analysis (RDA)[24], to examine how biotic and abiotic variables structured the one-hour-averaged VOC mixing ratios, which integrate marine and non-marine sources and sinks. This approach addresses a gap in marine VOC research[4]: the absence of integrated datasets linking atmospheric composition to coupled biotic and abiotic controls. The RDA correlation biplot (Fig. 2a) reveals the dominant patterns of marine atmospheric VOC variability constrained by these drivers.

RDA1 axis (19.4% of constrained variance) defines a temperature-driven stratification-productivity-carbon gradient, where surface temperature, thermal stratification, Chlorophyll *a*, and pCO_2 covary with phytoplankton biomass. Negative scores denote warm, stratified, productive waters with strong CO2 drawdown, conditions yielding maximum mixing ratios for most VOCs (Fig. 2). Positive scores indicate cooler, well-mixed states with elevated pCO_2, where aromatic and nitrile compounds prevail. RDA2 (9.7%) primarily reflects wind direction and salinity variation, separating Dinophyceae-dominated, higher-salinity waters from Cyanophyceae- and Prasinophyceae-enriched conditions. Phytoplankton groups show distinct environmental associations: Cyanophyceae and Prasinophyceae (which includes other small nanophytoplankton; see Methods) co-occur under stratified conditions, collectively contributing to elevated Chl-a. Euglenophyceae, Chlorophyceae, and Cryptophyceae also associate with stratified waters (negative RDA1) but show weaker or variable RDA2 loadings. Dinophyceae correlate with higher salinity and specific wind regimes, likely reflecting upwelling or advection of subsurface waters. Bacillariophyceae and Chrysophyceae show diffuse loadings across higher-order axes and do not strongly align with the primary environmental gradients.

VOC composition tracked an ecosystem gradient: a diagonal trajectory in ordination space links the progression from warm, stratified, phytoplankton-dominated surface waters (early campaign, negative RDA1) toward cooler, less productive, more physically mixed conditions (late campaign, positive RDA1), yielding two discrete clusters of m/z features. This chemical reorganization across the environmental gradient demonstrates that marine atmospheric VOCs act as sensitive indicators of ecosystem state transitions[25].

After assigning m/z features to chemical groups (Methods), we examined their constrained loadings. Organosulfurs (C□H□Sz), such as DMS (m/z 63.027) and methanethiol (m/z 49.005), project diagonally,

toward stratified, biomass-rich conditions characterized by cyanobacteria-dominated communities (Fig. 2b). These organosulfurs derive from phytoplankton-synthesized DMSP and its microbial transformation[26–28]. Although prymnesiophytes, chrysophytes, pelagophytes, and dinoflagellates typically dominate marine DMSP production (with cyanobacteria contributing minimally)[26,28], our results show strong associations with cyanobacteria-dominated waters. Despite this taxonomic discrepancy, atmospheric organosulfur levels closely track the oceanic biological activity.

Oxygenated compounds, including oxygenated VOCs (OVOCs; $C_xH_yO_z$), nitrogen-containing oxygenated compounds ($C_xH_yN_aO_b$), and most hydrocarbons (C_xH_y, including isoprene m/z 69.073) dominate negative RDA1 loadings, aligning with surface water temperature and opposing wind speed. These compounds show decreasing mixing ratios from early to late campaign, suggesting declining inputs from local and regional sources such as sea to air emissions, shipping, and terrestrial outflow[29,30], and/or increasing dilution from seasonal boundary layer deepening[31]. Substantial RDA2 variability indicates compound-specific variability in sources, atmospheric processing, or air-sea exchange. Aromatic hydrocarbons and nitrogen-containing VOCs (particularly acetonitrile; m/z 42.022) load on positive RDA1 and negative RDA2, decoupled from most other VOC groups, suggesting distinct atmospheric controls. Their mixing ratios increased during the late campaign; for acetonitrile, predominantly of non-marine origin, this pattern likely indicates changing advective regimes[32].

air-sea VOC fluxes were dominated by organosulfur and oxygenated compounds

We resolved three-hourly eddy-covariance fluxes for 48 quality-filtered VOC masses from the marine footprint (Methods; Fig. 3).Early in the campaign, organosulfurs dominate net emission, primarily driven by DMS (m/z 63.027; mean 5.9 ± 6.7 μmol m^{-2} d^{-1}, n=125, peaking at 40.3 μmol m^{-2} d^{-1} in late July). These fluxes are consistent with eddy covariance measurements over biologically productive waters in the North Atlantic[33], Southwest Pacific[34], and UK coastal waters[15] (mean DMS fluxes 3–18 μmol m^{-2} d^{-1}). The DMS:methanethiol flux ratio (m/z 63.027/49.005) averaged 9.9 ± 5.5 (median = 8.1, range = 1.3-22.9, n=59), comparable to reported oceanic values[7]. The two compounds were strongly correlated (R^2 = 0.82, slope = 14.0), with a steeper slope than previously observed in coastal waters[17]. Emissions then decline to near-zero despite intermittent windy periods, indicating water-side source limitation rather than air-side kinetic control in late season. The signal at m/z 126.968, tentatively dimethyl trisulfide (DMTS; mean 0.49 ± 0.30 μmol m^{-2} d^{-1}, n=30), showed weaker correlation with DMS (R^2 = 0.36) and emerged more prominently in mid-August, suggesting a decoupled or secondary sulfur source, possibly from eukaryotic microalgae (i.e. non-cyanobacterial algae)[35,36]. Overall, organosulfur emissions track atmospheric mixing ratios closely (R^2 = 0.67 for DMS), indicating direct coupling to water-side biological production.

In contrast, several oxygenated VOCs persistently deposited throughout the campaign. Acetone (m/z 59.049) dominates this air-to-sea flux signal (mean -9.1 ± 4.5 μmol m^{-2} d^{-1}, n=129, ranging from -23.4 to -1.2 μmol m^{-2} d^{-1}), followed by acetaldehyde (m/z 45.030; mean -7.5 ± 4.2 μmol m^{-2} d^{-1}, n=48), with both showing deposition strengthening during windy periods consistent with enhanced gas-transfer velocity or steeper air-sea concentration gradients[37]. Butanal (m/z 73.061; mean -0.29 ± 0.14 μmol m^{-2} d^{-1}, n=73) also showed persistent but smaller deposition. While some recent studies identify the ocean as a source of OVOCs in marine environments[23,38,39], our observations align with other findings in open ocean[40] and terrestrially influenced regions[15]. Unlike organosulfur fluxes, this deposition persisted across regimes, responding to short-term kinetic forcing rather than seasonal transitions. These fluxes showed negligible correlation with atmospheric mixing ratios ($R^2 < 0.06$), indicating that flux magnitude is controlled primarily by wind-driven gas transfer velocity rather than by atmospheric concentration variability. This pattern suggests either that water-side acetone concentrations remain consistently below atmospheric equilibrium or that they vary independently of atmospheric levels

Acetic acid (m/z 61.031), on the other hand, was predominantly emitted (mean 5.8 ± 2.5 μmol m^{-2} d^{-1}, n=53). Negligible during the late-July organosulfur peak, it became prominent in early August, with emission increasing (up to 12.5 μmol m^{-2} d^{-1}) during periods of elevated wind and mixing and dominated the emission budget in mid-to-late August as organosulfur fluxes declined. This provides rare direct flux constraints supporting the ocean as a net acetic acid source; however, our data cannot distinguish between direct emission and secondary production from marine precursors[41,42]. Formic acid (m/z 47.012) shows consistent deposition (mean -2.8 ± 0.9 μmol m^{-2} d^{-1}, n=31), with deposition weakly anticorrelated with atmospheric mixing ratios ($R^2 = 0.16$), in contrast to acetone and acetaldehyde, for which fluxes showed independence from atmospheric concentrations.

Nitrogen-containing features generally showed small-magnitude deposition, with acetonitrile (m/z 42.022) providing the clearest signal (mean -1.2 ± 0.5 μmol m^{-2} d^{-1}, n=83). This persistent air-to-sea flux became more prominent in the late season as organosulfur emissions waned, increasing from mid-August alongside rising atmospheric mixing ratios (consistent with RDA1 loadings, Fig. 2b). Intermittently, feature m/z 71.059 (tentatively butanenitrile; mean -0.76 ± 0.35 μmol m^{-2} d^{-1}, n=29) also showed deposition.

Isoprene (m/z 69.073) and monoterpenes (e.g., m/z 137.126) exhibited low-magnitude fluxes from the marine sector (isoprene: mean 0.54 ± 0.33 μmol m^{-2} d^{-1}, n=24; monoterpenes: mean 0.01 ± 0.24 μmol m^{-2} d^{-1}, n=4).Our isoprene fluxes fall between open-ocean observations (0.072 μmol m^{-2} d^{-1} during a North Atlantic transect in October–November 2013[43]) and more productive coastal waters (1.65 μmol m^{-2} d^{-1} at a UK coastal site in early May[15]), consistent with the Baltic Sea's intermediate productivity. Monoterpene fluxes align closely with North Atlantic values (0.04 μmol m^{-2} d^{-1})[43]. Other hydrocarbon features, such as m/z 83.085 (mean 0.54 ± 0.18 μmol m^{-2} d^{-1}, n=23) showing emission comparable to isoprene and m/z 77.036 (mean -0.50 ± 0.22 μmol m^{-2} d^{-1}, n=58) showing deposition, representing a

minor component of the total exchange budget. However, we note that highly reactive compounds (e.g., sesquiterpenes) may be underestimated due to losses during transport from the source to the analyser (including in the inlet line), while light hydrocarbons (e.g., ethane) were not detectable by our instrument.

Overall, the environmental gradients organizing mixing ratios, i.e., temperature, stratification, and wind-driven mixing, also structured fluxes. While organosulfur emissions tracked biological production under stratified conditions, OVOC deposition persists regardless of local atmospheric variations and was controlled by physical transfer velocity. Acetic acid proved exceptional, emerging as a dominant emission after the organosulfur peak. Nitrogen-compound deposition scales with atmospheric burden, increasing as late-season concentrations rise. This diversity created a clear temporal succession: organosulfur outgassing peaked in late July, followed by acetic acid emission in mid-to-late August, alongside sustained OVOC and nitrogen deposition throughout the transition from biologically productive to physically mixed conditions.

Drivers of VOC fluxes: biotic and abiotic variables

To examine how biotic and abiotic variables relate to air-sea VOC exchange, we applied conditional permutation importance analysis to Lasso regression models trained on fluxes of eight individual VOC compounds selected based on sufficient data and adequate performance (Methods; Fig. 4). Predictor variables mirrored those in redundancy analysis of the VOC mixing ratios.

Wind speed emerged as the dominant predictor across most models, consistent with its role governing gas transfer velocity[44]. Partial dependence analysis[45] confirmed monotonically increasing relationships between wind speed and flux magnitude for all compounds, indicating kinetic control dominates air-sea exchange regardless of flux direction. Wind direction also showed great importance for several models, consistent with wave development and fetch influences within the flux footprint. Notably, global radiation was not among the top predictors, suggesting that biological and physical oceanographic controls dominate over interfacial photochemistry at these temporal scales[3,10].

Among organosulfur compounds ($C_xH_yS_a$), DMS (m/z 63.027) fluxes appear source-limited and most strongly driven by Cyanophyceae biomass with secondary biotic contributions from Prasinophyceae and Euglenophyceae. This pattern aligns with observed DMS emission declines from early-season peaks (~40 μmol m^{-2} d^{-1}) to near-zero in late August despite sustained high winds, when cyanophyceae biomass declined, indicating reduced water-side production as the limiting factor. Wind speed remains a critical kinetic amplifier, but biological productivity sets the upper emission bound. Methanethiol (m/z 49.005) showed a distinct phytoplankton signature: Chrysophyceae and Bacillariophyceae emerged as significant predictors alongside wind speed and direction, suggesting different organosulfur compounds link to different phytoplankton community components. This distinction highlights that while these compounds may co-occur or align with similar broad environmental gradients (as seen in Fig. 3a), their specific biotic production pathways and dominant biological drivers can differ significantly.

Oxygenated VOC fluxes (C_xH_yO and $C_xH_yO_2$) are more closely tied to kinetic forcing. For acetone (m/z 59.049), wind speed dominated, followed by wind direction and relative humidity, consistent with increased deposition during high wind episodes. Although three phytoplankton classes (Chrysophyceae, Prasinophyceae, Bacillariophyceae) showed significant contributions, their effect sizes were minor relative to abiotic drivers. Butanal (m/z 73.061) showed similar dominance by wind speed and direction, with Prasinophyceae as the only significant biotic predictor (negative association). Overall weak biotic predictor importances for C_xH_yO compounds suggests that air-to-sea transfer is governed primarily by atmospheric supply and physical transfer rather than water-side biological consumption[46].

Among $C_xH_yO_2$ compounds, acetic acid (m/z 61.031) is driven predominantly by wind speed, with relative humidity as a significant secondary predictor and negligible biotic contributions. This sensitivity to relative humidity likely reflects acetic acid's high water solubility and consequent removal via fog scavenging and aerosol uptake[30]. Formic acid (m/z 47.012) showed weaker model performance and was most strongly associated with wind speed.

Acetonitrile (m/z 42.022), the only nitrogen-containing compound ($C_xH_yN_a$) with sufficient flux data, showed dominant wind speed control with secondary wind direction contribution, but negligible biotic predictors, consistent with atmospheric deposition from continental sources (e.g., biomass burning[32]) overwhelming any marine biological source or sink. The only hydrocarbon deposition analyzed (m/z 77.036) similarly showed wind speed as the sole significant predictor, suggesting flux governed entirely by physical gas exchange.

Bulk Chlorophyll *a* showed negligible predictive power across models. While Chlorophyll *a*'s failure to predict DMS has been recognized[47], our results extend this limitation to a broader VOC suite, reinforcing that community composition, rather than total biomass, governs VOC production[23].

Conclusions and outlook

By coupling continuous PTR-TOF-MS eddy covariance measurements with taxonomically resolved phytoplankton and hydrographic observations, we demonstrate that marine VOC exchange is chemically diverse and dynamically reconfigurable on event-to-season timescales. Environmental gradients that structure atmospheric VOC composition also drive air-sea fluxes, and their influence partitions by chemical group: organosulfur emissions are source-limited by phytoplankton community composition (outperforming bulk Chlorophyll *a* as a predictor), declining to near-zero despite favorable gas-transfer conditions as cyanobacteria biomass declines, whereas oxygenated VOC deposition persists throughout, governed primarily by kinetic forcing. Notably, acetic acid emerges as the second-largest emission contributor, illustrating how chemically broad observations reveal previously underappreciated fluxes.

Measurement uncertainties (including uncalibrated quantification, potential isomeric ambiguities, inlet losses, and high-frequency attenuation) motivate conservative flux interpretation and continued refinement. Nonetheless, our approach captures flux reorganization and environmental coupling that

targeted campaigns cannot resolve, providing a pathway to constrain chemically broad marine VOC budgets. Future efforts should prioritize water-side concentration measurements, extend observations to open-ocean regimes and the sea-surface microlayer, and resolve microbial community and physiological mechanisms linking marine metabolism to VOC production, advancing predictive understanding of how marine ecosystems regulate atmospheric composition under changing climate.

Methods

Measurement site and setup

Measurements were conducted at Utö Marine and Atmospheric Research Station[48] (maintained by the Finnish Meteorological Institute and the Finnish Environment Institute at the southern edge of the Archipelago Sea, Baltic Sea; 59°46'49.4"N, 21°21'13.0"E) from July to September 2024. The eddy covariance mast is sited on the exposed western shore, with a horizontal distance of ~4 m from the shoreline, providing direct marine fetch under onshore winds[49]. Air was sampled adjacent to the 3-D sonic anemometer (Metek uSonic-3) mounted at 11.5 m a.m.s.l. (mean sea level at Utö varies approximately ±0.5 m), minimizing inlet-anemometer separation (vertical separation: 20 cm, lateral separations: 10 cm). Sample air was drawn through a 40 m PFA inlet (OD 1/2 in, ID 3/8 in) heated to 40 °C to suppress condensation and wall interactions. A primary pump maintained 40 L min^{-1} through the main line, from which a subsample was delivered to the PTR-TOF-MS, housed inside a hut approximately 15 meters from the mast. A PTFE membrane filter was installed upstream of the instrument; no dryer was used to avoid contamination and artifacts. The mean residence time from inlet tip to detector, inferred from covariance-lag analysis, was ~8.9 s and remained stable throughout the campaign. To ensure a marine source area, analyses were restricted to periods with wind direction within 210–330°, which encompassed approximately half of the campaign duration. VOCs were measured with an IONICON PTR-TOF-MS T1000 ultra operating in H3O+ mode. Drift tube parameters were: pressure 2.3 mbar, temperature 60 °C, voltage 505 V, yielding E/N ≈ 108 Td. Calibrations were performed at the beginning and at the end of the campaign at the measurement site using a multicomponent standard containing methanol (m/z 33.033), acetonitrile (42.034), acetaldehyde (45.033), acetone (59.049), isoprene (69.070), butanal (73.065), benzene (79.054), toluene (93.070), xylene (107.086), and monoterpenes (137.132). These are protonated masses; measured m/z values may differ slightly. All m/z values reported throughout this study represent measured masses from the PTR-TOF-MS rather than theoretical protonated masses.

Auxiliary variables and phytoplankton biomass data

Hydrographic and phytoplankton observations at Utö station were conducted using a continuous seawater pumping system. The water inlet is located at the footprint of the flux measurement tower, 250 m offshore. The system is described in detail by Honkanen *et al.*[50] and Kraft *et al.*[51,52]. Briefly, water is taken at 4.5 m depth using an underwater pump, and pumped to the measuring cabin (Fig. 1c, orange

dashed box) at a rate of 50-60 L min^{-1} with a residence time of approximately 6 min in the pipe system. In the cabin, water is distributed continuously through various flowthrough sensors. Temperature and salinity were measured with a thermosalinograph (SBE45MicroTSG, Sea-Bird Scientific), and a correction for temperature is applied according to Honkanen *et al.*[50,53] as the temperature changes slightly when water flows from a pump to the cabin. Chlorophyll *a* fluorescence was measured with a Wetlabs ECO FLNTU fluorometer (Sea-Bird Scientific) system, adjusted based on calibration with filtered Chlorophyll *a*[52]. Phytoplankton community structure was measured using Imaging FlowCytobot (IFCB) connected to the flowthrough system, processing a 5-mL sample every ~20 min. IFCB takes images of Chlorophyll *a* containing phytoplankton particles with a size range from single cells with a diameter of ~5 µm to cyanobacteria with a filament length of ~300 µm. The images were classified using a Convolutional Neural Network algorithm[54], but with an updated classifier version. For this study, the classified taxonomic groups/taxa were aggregated into group level. The class/group-specific accuracies for automated classification are reported in Kraft *et al.*[54]. Automated classification at the group level performs well, with one exception: Prasinophyceae also contains other nanophytoplankton and can be used as an indicator of unidentified nanophytoplankton. Prasinophyceae are partly correctly classified; therefore, this category includes both correctly identified Prasinophyceae and other small unidentified phytoplankton.

The partial pressure of carbon dioxide (pCO_2) was measured using a non-dispersive infrared gas analyzer (LI-840A, LI-COR) in a SuperCO2 system (Sunburst Sensors), which was connected to the flow-through system[49]. Calibrations, corrections and drift compensations were done according to Honkanen *et al.*[50].

The meteorological variables (air temperature, humidity, global radiation, wind speed and direction) were measured at the FMI's automatic weather station, located on the southeastern part of the island. The height of the wind measurement is 25 m a.m.s.l. and the ground is relatively flat with rocks and a few small shrubs. Temperature and relative humidity are measured at 8 m a.m.s.l. and solar radiation at 10 m a.m.s.l.

Full list of continuous marine, atmospheric and electromagnetic observations made at Utö is available at https://en.ilmatieteenlaitos.fi/uto-observations.

PTR-TOF-MS preprocessing and quantification

Raw spectra were processed with PTRwid (v003 released March 7th, 2018) for peak detection, mass-scale calibration, baseline correction, and determination of peak shape/resolution, yielding a unified, campaign-wide peak list. For each retained peak, PTRwid[55] exported a time series of raw signals in counts per second (cps). The mixing ratios for each identified mass were then quantified using:

$$\mathrm{VMR_M(ppbv)} = \frac{\mathrm{i\left(MH^+\right)}}{\mathrm{Tr\left(MH^+\right)}} \cdot \frac{\mathrm{Tr\left(H_3O^+\right)}}{\mathrm{i\left(H_3O^+\right)}} \cdot \frac{10^9 \cdot \mathrm{U_{drift}} \cdot \mathrm{K_0^{H_3O^+}} \cdot \mathrm{V_0} \cdot \mathrm{p_0^2} \cdot \mathrm{T_{drift}^2}}{\mathrm{k_M} \cdot \mathrm{L^2} \cdot \mathrm{p_{drift}^2} \cdot \mathrm{N_A} \cdot \mathrm{T_0^2}}$$

The quantification uses drift-tube parameters (temperature, pressure, electrical potential) and a transmission factor Tr(m/z) that accounts for TOF mass-dependent efficiency, taken from the instrument's transmission curve. To address partially resolved ions that escaped automated detection, we complemented PTRwid with targeted inspection and deconvolution. Visual screening for asymmetric or shouldered peaks (In particular for acetaldehyde near nominal m/z 45) was followed by constrained multi-peak fits in Ionicon PTR-Viewer (v 3.4.5) using the campaign-specific peak shape determined by PTRwid. Components were accepted only if they (i) matched expected exact masses within the campaign-mean mass-accuracy tolerance, and (ii) showed physically plausible temporal behavior. Accepted components were added to the unified mass list and quantified with the same formulation as above. For well-resolved, high-SNR compounds (e.g., acetone m/z 59.049, DMS m/z 63.027), cross-software checks showed PTRwid and PTR-Viewer gave consistent mixing ratios and 30-min fluxes.

For peaks represented in the multicomponent calibration standard, VOC-specific calibration factors were obtained by regressing PTRwid-computed mixing ratios against standard concentrations during the beginning and end calibrations; slopes were averaged when drift was negligible or linearly interpolated in time otherwise. For compounds without standards, signals were treated as semi-quantitative. In addition, parent compounds and their characteristic fragments were summed for flux calculations: m/z 137.126 + 81.071 and m/z 61.031 + 43.013, based on high temporal correlation and consistency with literature fragmentation patterns.

Because in-campaign zero air was unavailable, we relied on the standard PTR-TOF mixing-ratio formulation to stabilize the time series against instrument-state variability. In this formulation, the transmission factor corrects the analyte signal for mass-dependent efficiency, and the equation above provides reagent-ion normalization to remove first-order sensitivity changes driven by fluctuations in the reagent-ion intensity. While these terms do not substitute for background subtraction, they reduce short-term gain variability and mass bias so that the variability used in downstream analyses reflects marine atmospheric signals. Accordingly, multivariate analyses (RDA) used z-scored variables that are insensitive to constant offsets, and eddy-covariance fluxes were computed from 30-min fluctuations about the block mean, which remove steady background contributions within each averaging interval. These methodological choices ensure that the reported patterns and flux estimates are robust to the absence of zero-air background measurements.

We did not derive humidity-resolved sensitivities because we lacked controlled injections of standards across a range of humidities. Instead, we assessed empirical RH dependence by regressing mixing ratios against ambient RH for all retained VOC masses. The vast majority of compounds showed negligible correlation with RH ($R^2 < 0.05$), with only a few compounds exhibiting modest trends ($R^2 \leq$

0.12). Given the absence of systematic, compound-general humidity effects, we treat humidity as a contributor to sensitivity uncertainty rather than applying explicit corrections.

VOC data quality control and compound selection

VOC mixing ratios measured at 10 Hz were resampled to 1-hour temporal resolution and subjected to a multi-stage quality control pipeline. First, outliers were removed using a rolling despiking algorithm (window = 3 hours). Signal quality was then quantified via wavelet-based signal-to-noise ratio (SNR) analysis. Compound filtering applied multiple objective criteria sequentially: (1) detection threshold: compounds with 95th percentile concentrations below 0.025 ppbv were excluded to remove near-detection-limit signals; (2) SNR threshold (>0.1) and temporal variability threshold (interquartile range ratio >0.02), set as permissive criteria to avoid over-filtering based on dataset-dependent statistical metrics, instead prioritizing the detection limit constraint. In practice, the detection limit criterion was the primary filter, removing 116 of 170 excluded compounds, while SNR and variability thresholds excluded no additional compounds. Masses corresponding to known instrument contaminants (e.g., water clusters, reagent ion clusters), inorganic ions (metals, halogens), and isotopes of major compounds (e.g., DMS and acetone) were manually excluded (n=30). This filtering reduced the dataset from 244 to 74 compounds, with despiking affecting 0.4% of data points. A complete list of all detected mass peaks with their filtering outcomes and applied criteria is provided in Supplementary Table 1.

Putative chemical identities were assigned by matching experimental masses to the GLOVOCS database (enhanced with Ionicon instrument-specific entries) within a ±0.015 Da tolerance window. For each mass, up to three closest matches were retrieved along with chemical formulas and hierarchical classifications (class, superclass, subclass). Of the 74 quality-controlled compounds, 48 yielded confident database matches and were retained for multivariate analysis. The final compound set spanned organosulfurs, terpenoids, oxygenated VOCs, and nitriles; a complete list with tentative assignments is provided in Supplementary Table 1.

As a final validation step, we performed eddy-covariance-informed diagnostics to confirm that no compounds exhibiting clear flux signals were inadvertently excluded. Time-lag distributions between individual VOC signals and vertical wind velocity were computed over a ±15 s window; compounds with physically consistent lag structure (e.g., DMS and acetone both peaked near 8.9 s) and unimodal hourly flux distributions indicating coherent emission or deposition were verified to be retained in the filtered dataset.

Redundancy analysis (RDA)

We related one-hour averaged marine atmospheric VOC composition to co-located abiotic and biotic variables using redundancy analysis (RDA), a constrained ordination method. Prior to analysis, Moderately-to-highly skewed features (|skewness| > 0.75) in both response (Y: 48 VOC m/z features;

Supplementary Table 1) and predictor (X: 20 environmental variables; Fig. 2a) matrices were transformed using the Yeo-Johnson power transformation, followed by z-score standardization. RDA was performed using the Python scikit-bio implementation with correlation biplot scaling (scaling = 2) to emphasize relationships among VOCs and environmental drivers.

The full model incorporating all 20 predictors ($R^2 = 0.787$, $p = 0.001$) was used for final interpretation and visualization. Forward selection with permutation testing ($\alpha = 0.05$, 999 permutations) was performed as a diagnostic check to confirm that the diffuse variance distribution across RDA axes (29 axes required for 80% of constrained variance) reflected inherent dataset structure rather than predictor multicollinearity or overfitting. This indicated that the relatively low percentage of constrained variance captured by the first few RDA axes arises from genuinely multi-dimensional VOC vs. environment relationships, rather than from collinearity among predictors or overfitting.

Statistical significance of the global RDA model was assessed via permutation tests (999 permutations) by comparing the observed R^2 to a null distribution generated by randomly permuting response matrix rows. Constrained variance explained by each RDA axis was calculated as the proportion of total eigenvalue sum.

For visualization, environmental vectors in the RDA biplot (Fig. 2a) were displayed as correlations between standardized predictor variables and sample scores on the plotted axes. VOC loadings (Fig. 2b) were displayed as compounds scores on the ordination axes, with arrow lengths representing the strength of each VOC's association with the displayed RDA dimensions. VOC m/z features were assigned to chemical groups based on tentative molecular formulas (VOCs filtering and labeling) to assess compositional patterns across ordination space.

Eddy covariance calculations

Vertical fluxes of VOCs were quantified using the eddy covariance method implemented in EddyPro software (v7.0.9; LI-COR Biosciences). Fluxes were derived from 10 Hz vertical wind speed and VOC mixing ratio time series, over 30-minute intervals, employing block average detrending and a double rotation of the coordinate system to align vertical velocities with the mean flow. To accurately determine the appropriate time lag between the signals, a two-step covariance maximization procedure was employed. First, a covariance search within a broad window (±15 s) was conducted for all VOC masses without prior filtering. High-intensity compounds, such as Acetone and DMS, exhibited consistent covariance peaks with a characteristic system lag of approximately 8.9 seconds, corresponding to the transit time through the 40-meter inlet line (see Extended Data Fig. 1, which illustrates the distribution of lag times for four selected compounds as an example). This physical lag time serves as a qualitative indicator of the system's detection limit: compounds with signals too weak to produce a detectable covariance peak were flagged as having no resolvable flux signal. To validate this approach, we confirmed that our quality-control pipeline (described in VOC data quality control and compound selection) did not inadvertently exclude compounds exhibiting significant flux signals; we observed

perfect overlap between the two filtering methods, confirming the robustness of our initial quality-control approach. In the second step, this physically determined lag (8.9 s) was applied as a fixed, constant lag for all filtered VOCs, enabling flux calculations across the retained compound suite.

High-frequency spectral losses, arising from attenuation in the sampling line and sensor separation, were corrected using analytical transfer functions, with low-pass filtering corrections applied according to the Massman fully analytical method[56,57] as implemented in EddyPro. Fitted Massman transfer function models and ensemble-averaged cospectral densities, illustrating the spectral transfer characteristics and frequency-dependent attenuation for both unstable and stable atmospheric conditions, are presented in Extended Data Fig. 2. Quality control (used Mauder and Foken 0-1-2 system) included stationarity and turbulence tests, and only data segments passing these tests with QC flags=0 (highest quality) were retained for further flux calculations.

Half-hourly fluxes, filtered for quality, were subsequently resampled to multiple temporal resolutions. A minimum of 50% of valid half-hour observations was required for aggregation to 3-hour windows. Flux uncertainties were computed by propagating the standard error of the mean and EddyPro's estimated random errors in quadrature, with

the total uncertainty given by: $\sigma_{\text{total}} = \sqrt{\text{SEM}^2 + \sigma_{\text{RE}}^2}$. To ensure statistical robustness, only aggregated fluxes where the magnitude exceeded twice the total uncertainty ($|\text{flux}|/\sigma_{\text{total}} \geq 2$) were considered significant.

Regression analysis and conditional permutation importance

To examine relationships between biotic and abiotic variables and air-sea VOC exchange, we applied Lasso (Least Absolute Shrinkage and Selection Operator) regression with conditional permutation importance analysis. Models were trained separately on compound-level VOC fluxes for eight individual compounds, selected based on sufficient valid flux data points and adequate regression performance. We used the 3-hour bins employed in temporal flux analysis. Predictor variables mirrored those used in RDA analysis of VOC mixing ratios (Fig. 2a). Moderately-to-highly skewed features (|skewness| > 0.75) underwent Yeo-Johnson power transformation prior to standardization (zero mean, unit variance) applied to all predictors.

Lasso regression was selected over Ridge and elastic net alternatives based on higher out-of-bag validation performance. The regularization parameter (α) was optimized via two-stage random search (Stage 1: 40 iterations over $\alpha \in [0.005, 0.2]$; Stage 2: 30 iterations in refined range) using 4-fold stratified cross-validation based on target quantile bins to maintain flux distribution balance. To obtain robust performance estimates for interpreting predictor importance, models were validated using stratified

bootstrap resampling (1,000 iterations). Bootstrap samples were stratified by flux quantiles to ensure balanced flux distributions, with out-of-bag samples serving as validation sets.

To quantify predictor contributions while accounting for feature correlations, we implemented conditional permutation importance analysis. For each predictor, values were permuted within clusters of similar observations to preserve the correlation structure with other predictors. Specifically, samples were partitioned into k = 10 clusters via K-means clustering based on all non-permuted features, and permutation occurred only within each cluster. This approach prevents inflated importance estimates for correlated predictors that would arise from naive permutation breaking natural feature dependencies. Circular variables (wind direction) were decomposed into sine and cosine components and treated as grouped features during permutation. Similarly, global radiation was represented as daily values and day-night binary components. Importance was quantified as the decrease in R^2 after permutation, averaged over 100 permutation repeats per predictor group.

Bootstrap confidence intervals (95%) for importance values were derived from 100 bootstrap iterations, each involving model retraining and permutation importance calculation. Statistical significance was assessed via one-tailed permutation tests (H_0: importance = 0 vs. H_1: importance > 0), with significance thresholds at $p < 0.05$, $p < 0.01$, and $p < 0.001$. Effect direction (increasing, decreasing, or no effect) was determined using partial dependence analysis. For each predictor, we computed averaged partial dependence plots (PDPs) and assessed monotonicity using Spearman rank correlation (ρ) between predictor values and partial dependence. Effects were classified as increasing if $\rho > 0.1$ ($p < 0.05$), decreasing if $\rho < -0.1$ ($p < 0.05$), or negligible otherwise. For grouped circular features (sine/cosine pairs), effect direction was based on the component with greater partial dependence range, with warnings issued when components showed opposing effects. All analyses were conducted in Python using scikit-learn (v1.5.2) for regression modeling and custom implementations for conditional permutation importance.

Declarations

Use of AI

Large language models (ChatGPT/Claude) were used to assist with language editing, including grammar checking and suggesting alternative formulations. All scientific content and interpretations remain the sole responsibility of the authors.

Data availability

The datasets generated and analyzed during this study will be available in the Zenodo repository (https://zenodo.org/) upon publication, with a DOI to be assigned.

Acknowledgments

This project was supported by the Danish National Research Foundation within the Center for Volatile Interactions (VOLT, DNRF168). T.H. was supported by the Strategic Research Areas BECC (Biodiversity and Ecosystem services in a Changing Climate) and MERGE (ModElling the Regional and Global Earth system) funded by the Swedish Government. Support from the Research Council of Finland was provided through projects FASTVISION-plus (Grant No. 339355; K.K. and J.S.) and MAVOC (Grant Nos. 361298 and 361299; K.K., J.S., M.H., L.L., K.S., and H.H.). M.H., L.L., and K.S. also received support from AQUARIUS, funded by the European Union's Horizon Europe Framework Programme for Research and Innovation (Grant No. 101130915). This study was conducted using research infrastructure provided by the Finnish Marine Research Infrastructure (FINMARI) consortium. We thank Ismo and Brita Willström for their invaluable support during measurements at Utö Atmospheric and Marine Research Station.

Author information

Authors and Affiliations

Department of Biology, University of Copenhagen, Denmark

Mehrshad Foroughan, Riikka Rinnan

Department of Earth and Ecosystem Sciences, Lund university, Sweden

Thomas Holst

Research Infrastructure, Finnish Environment Institute

Kaisa Kraft, Jukka Seppälä

Meteorological and Marine Research Programme, Finnish Meteorological Institute

Martti Honkanen, Lauri Laakso, Ken Stenbäck

Atmospheric Composition Unit, Finnish Meteorological Institute

Heidi Hellén

GEOMAR Helmholtz-Centre for Ocean Research Kiel

Christa Marandino

Contributions

Conceptualization: M.F., R.R.; Methodology: T.H., M.F., K.K., J.S.; Software: M.F.; Investigation: T.H., M.F., K.K., M.H., L.L., H.H., J.S., K.S.; Formal analysis: M.F., K.K., M.H.; Data curation: M.F., K.K, M.H.; Visualization: M.F.; Writing – original draft: M.F.; Writing – review & editing: M.F., T.H., K.K., M.H., L.L., H.H., J.S., K.S., C.M., R.R.; Resources: L.L., R.R.; Funding acquisition: R.R.; Supervision: R.R.; Project administration: M.F., L.L., R.R.

Corresponding authors

Correspondence to Mehrshad Foroughan and Riikka Rinnan.

References

1. Liss, P. S. *et al.* Short-Lived Trace Gases in the Surface Ocean and the Atmosphere. in *Ocean-Atmosphere Interactions of Gases and Particles* (eds Liss, P. S. & Johnson, M. T.) 1–54 (Springer, Berlin, Heidelberg, 2014). doi:10.1007/978-3-642-25643-1_1.
2. Tinel, L. *et al.* Impacts of ocean biogeochemistry on atmospheric chemistry. *Elementa: Science of the Anthropocene* **11**, 00032 (2023).
3. Novak, G. A. & Bertram, T. H. Reactive VOC production from photochemical and heterogeneous reactions occurring at the air–ocean interface. *Acc. Chem. Res.* **53**, 1014–1023 (2020).
4. Halsey, K. H. & Giovannoni, S. J. Biological controls on marine volatile organic compound emissions: A balancing act at the sea-air interface. *Earth-Science Reviews* **240**, 104360 (2023).
5. Legg, S. IPCC, 2021: Climate change 2021-the physical science basis. *Interaction* **49**, 44–45 (2021).
6. Marandino, C. A., De Bruyn, W. J., Miller, S. D. & Saltzman, E. S. Eddy correlation measurements of the air/sea flux of dimethylsulfide over the North Pacific Ocean. *Journal of Geophysical Research: Atmospheres* **112**, (2007).
7. Rocco, M. *et al.* Air-Sea fluxes of dimethyl sulphide and methanethiol in the South-West Pacific. *EGUsphere* 1–31 (2023) doi:10.5194/egusphere-2023-516.
8. Joge, S. D. *et al.* Dimethyl sulfide (DMS) climatologies, fluxes, and trends – Part 2: Sea–air fluxes. *Biogeosciences* **21**, 4453–4467 (2024).
9. Broadgate, W. J., Liss, P. S. & Penkett, S. A. Seasonal emissions of isoprene and other reactive hydrocarbon gases from the ocean. *Geophysical Research Letters* **24**, 2675–2678 (1997).
10. Ciuraru, R. *et al.* Unravelling New Processes at Interfaces: Photochemical Isoprene Production at the Sea Surface. *Environ. Sci. Technol.* **49**, 13199–13205 (2015).
11. Carpenter, L. J. *et al.* Uptake of methanol to the North Atlantic Ocean surface. *Global Biogeochemical Cycles* **18**, (2004).

12. Yang, M. *et al.* Atmospheric deposition of methanol over the Atlantic Ocean. *Proceedings of the National Academy of Sciences* **110**, 20034–20039 (2013).
13. Marandino, C. A., De Bruyn, W. J., Miller, S. D., Prather, M. J. & Saltzman, E. S. Oceanic uptake and the global atmospheric acetone budget. *Geophysical Research Letters* **32**, (2005).
14. Yang, M., Blomquist, B. W. & Nightingale, P. D. Air-sea exchange of methanol and acetone during HiWinGS: Estimation of air phase, water phase gas transfer velocities. *Journal of Geophysical Research: Oceans* **119**, 7308–7323 (2014).
15. Phillips, D. P. *et al.* Air–sea exchange of acetone, acetaldehyde, DMS and isoprene at a UK coastal site. *Atmospheric Chemistry and Physics* **21**, 10111–10132 (2021).
16. Beale, R., Dixon, J. L., Arnold, S. R., Liss, P. S. & Nightingale, P. D. Methanol, acetaldehyde, and acetone in the surface waters of the Atlantic Ocean. *Journal of Geophysical Research: Oceans* **118**, 5412–5425 (2013).
17. Novak, G. A., Kilgour, D. B., Jernigan, C. M., Vermeuel, M. P. & Bertram, T. H. Oceanic emissions of dimethyl sulfide and methanethiol and their contribution to sulfur dioxide production in the marine atmosphere. *Atmospheric Chemistry and Physics* **22**, 6309–6325 (2022).
18. Lana, A. *et al.* An updated climatology of surface dimethlysulfide concentrations and emission fluxes in the global ocean. *Global Biogeochemical Cycles* **25**, (2011).
19. Mincer, T. J. & Aicher, A. C. Methanol Production by a Broad Phylogenetic Array of Marine Phytoplankton. *PLOS ONE* **11**, e0150820 (2016).
20. Park, J.-H. *et al.* Eddy covariance emission and deposition flux measurements using proton transfer reaction – time of flight – mass spectrometry (PTR-TOF-MS): comparison with PTR-MS measured vertical gradients and fluxes. *Atmos. Chem. Phys.* **13**, 1439–1456 (2013).
21. Wohl, C. *et al.* Marine biogenic emissions of benzene and toluene and their contribution to secondary organic aerosols over the polar oceans. *Science Advances* **9**, eadd9031 (2023).
22. Marandino, C. A., De Bruyn, W. J., Miller, S. D. & Saltzman, E. S. Open ocean DMS air/sea fluxes over the eastern South Pacific Ocean. *Atmospheric Chemistry and Physics* **9**, 345–356 (2009).
23. Rocco, M. *et al.* Fluxes of Biogenic and Oxygenated VOCs From In Situ Mesocosm Studies of Seawaters From the South-West Pacific Ocean. *Journal of Geophysical Research: Atmospheres* **130**, e2024JD043056 (2025).
24. Canonical analysis. in *Developments in Environmental Modelling* vol. 24 625–710 (Elsevier, 2012).
25. Saha, M. & Fink, P. Algal volatiles – the overlooked chemical language of aquatic primary producers. *Biological Reviews* **97**, 2162–2173 (2022).
26. McParland, E. L. & Levine, N. M. The role of differential DMSP production and community composition in predicting variability of global surface DMSP concentrations. *Limnology and Oceanography* **64**, 757–773 (2019).
27. Zhao, Y., Schlundt, C., Booge, D. & Bange, H. W. A decade of dimethyl sulfide (DMS), dimethylsulfoniopropionate (DMSP) and dimethyl sulfoxide (DMSO) measurements in the

southwestern Baltic Sea. *Biogeosciences* **18**, 2161–2179 (2021).

28. Wang, J. *et al.* Alternative dimethylsulfoniopropionate biosynthesis enzymes in diverse and abundant microorganisms. *Nat Microbiol* **9**, 1979–1992 (2024).
29. Wang, J. *et al.* The role of oceanic ventilation and terrestrial outflow in atmospheric non-methane hydrocarbons over the Chinese marginal seas. *Atmospheric Chemistry and Physics* **24**, 8721–8736 (2024).
30. Derstroff, B. *et al.* Volatile organic compounds (VOCs) in photochemically aged air from the eastern and western Mediterranean. *Atmos. Chem. Phys.* **17**, 9547–9566 (2017).
31. Rautiainen, L. *et al.* Marine Atmospheric Ducting Statistics Based on 2 Years of Coastal Surveillance Radar Observations. *Journal of Applied Meteorology and Climatology* **64**, 63–76 (2025).
32. de Gouw, J. A. *et al.* Emission sources and ocean uptake of acetonitrile (CH3CN) in the atmosphere. *Journal of Geophysical Research: Atmospheres* **108**, (2003).
33. Marandino, C. A., De Bruyn, W. J., Miller, S. D. & Saltzman, E. S. DMS air/sea flux and gas transfer coefficients from the North Atlantic summertime coccolithophore bloom. *Geophysical Research Letters* **35**, (2008).
34. Smith, M. J. *et al.* Gradient flux measurements of sea–air DMS transfer during the Surface Ocean Aerosol Production (SOAP) experiment. *Atmospheric Chemistry and Physics* **18**, 5861–5877 (2018).
35. Achyuthan, K. E., Harper, J. C., Manginell, R. P. & Moorman, M. W. Volatile Metabolites Emission by In Vivo Microalgae—An Overlooked Opportunity? *Metabolites* **7**, 39 (2017).
36. Patidar, S. K. Metabolic interactions between microalgae and bacteria: Multifunctional ecological interplay and environmental applications. *Algal Research* **86**, 103904 (2025).
37. Garbe, C. S. *et al.* Transfer Across the Air-Sea Interface. in *Ocean-Atmosphere Interactions of Gases and Particles* (eds Liss, P. S. & Johnson, M. T.) 55–112 (Springer, Berlin, Heidelberg, 2014). doi:10.1007/978-3-642-25643-1_2.
38. Kilgour, D. B., Novak, G. A., Claflin, M. S., Lerner, B. M. & Bertram, T. H. Production of oxygenated volatile organic compounds from the ozonolysis of coastal seawater. *Atmospheric Chemistry and Physics* **24**, 3729–3742 (2024).
39. Brewer, J. F. *et al.* Evidence for an oceanic source of methyl ethyl ketone to the atmosphere. *Geophysical Research Letters* **47**, e2019GL086045 (2020).
40. Yang, M. *et al.* Air–sea fluxes of oxygenated volatile organic compounds across the Atlantic Ocean. *Atmospheric Chemistry and Physics* **14**, 7499–7517 (2014).
41. Paulot, F. *et al.* Importance of secondary sources in the atmospheric budgets of formic and acetic acids. *Atmospheric Chemistry and Physics* **11**, 1989–2013 (2011).
42. Lee, X. *et al.* Underrated primary biogenic origin and lifetime of atmospheric formic and acetic acid. *Sci Rep* **11**, 7176 (2021).
43. Kim, M. J. *et al.* Air-Sea exchange of biogenic volatile organic compounds and the impact on aerosol particle size distributions. *Geophysical Research Letters* **44**, 3887–3896 (2017).

44. Blomquist, B. W. *et al.* Wind speed and sea state dependencies of air-sea gas transfer: Results from the High Wind Speed Gas Exchange Study (HiWinGS). *Journal of Geophysical Research: Oceans* **122**, 8034–8062 (2017).
45. Hastie, T., Tibshirani, R. & Friedman, J. Chapter 10 Boosting and Additive Trees. in *The Elements of Statistical Learning: Data Mining, Inference, and Prediction* (eds Hastie, T., Tibshirani, R. & Friedman, J.) 337–387 (Springer, New York, NY, 2009). doi:10.1007/978-0-387-84858-7_10.
46. Moore, E. R., Weaver, A. J., Davis, E. W., Giovannoni, S. J. & Halsey, K. H. Metabolism of key atmospheric volatile organic compounds by the marine heterotrophic bacterium Pelagibacter HTCC1062 (SAR11). *Environmental Microbiology* **24**, 212–222 (2022).
47. Wang, W.-L. *et al.* Global ocean dimethyl sulfide climatology estimated from observations and an artificial neural network. *Biogeosciences* **17**, 5335–5354 (2020).
48. Laakso, L. *et al.* 100 years of atmospheric and marine observations at the Finnish Utö Island in the Baltic Sea. *Ocean Science* **14**, 617–632 (2018).
49. Honkanen, M. *et al.* Measuring turbulent CO_2 fluxes with a closed-path gas analyzer in a marine environment. *Atmospheric Measurement Techniques* **11**, 5335–5350 (2018).
50. Honkanen, M. *et al.* Interannual and seasonal variability of the air–sea CO_2 exchange at Utö in the coastal region of the Baltic Sea. *Biogeosciences* **21**, 4341–4359 (2024).
51. Kraft, K. *et al.* First Application of IFCB High-Frequency Imaging-in-Flow Cytometry to Investigate Bloom-Forming Filamentous Cyanobacteria in the Baltic Sea. *Front. Mar. Sci.* **8**, (2021).
52. Kraft, K. *et al.* Monitoring cyanobacteria blooms with complementary measurements – a similar story told using high-throughput imaging, optical sensors, light microscopy, and satellite-based methods. *Harmful Algae* **147**, 102865 (2025).
53. Honkanen, M. *et al.* The diurnal cycle of pCO_2 in the coastal region of the Baltic Sea. *Ocean Science* **17**, 1657–1675 (2021).
54. Kraft, K. *et al.* Towards operational phytoplankton recognition with automated high-throughput imaging, near-real-time data processing, and convolutional neural networks. *Front. Mar. Sci.* **9**, (2022).
55. Holzinger, R. PTRwid: A new widget tool for processing PTR-TOF-MS data. *Atmospheric Measurement Techniques* **8**, 3903–3922 (2015).
56. Massman, W. J. Reply to comment by Rannik on “A simple method for estimating frequency response corrections for eddy covariance systems”. *Agricultural and Forest Meteorology* **107**, 247–251 (2001).
57. Massman, W. J. A simple method for estimating frequency response corrections for eddy covariance systems. *Agricultural and Forest Meteorology* **104**, 185–198 (2000).

Figures

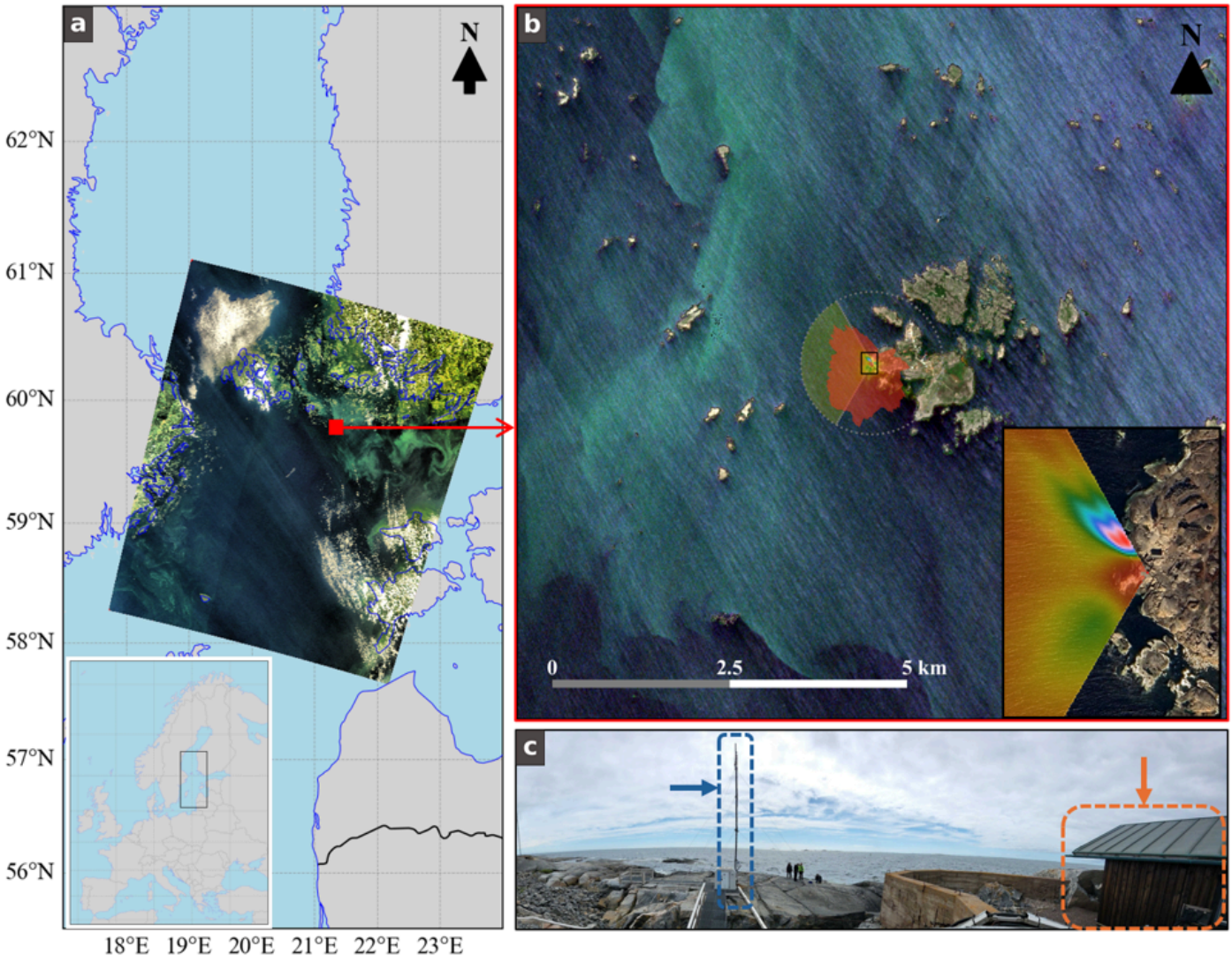


Figure 1

a) Sentinel-3 image (30 July 2024), showing cyanobacteria blooms (green swirls) in the Baltic Sea. A red rectangle marks Utö Island at the Archipelago Sea's outer edge; inset shows the location in Europe. b) Higher-resolution Sentinel-2 image from the same day. A black square marks the measurement site on Utö's western shore. The overlay displays the climatological flux footprint, with the marine sector used in this study (210-330°) highlighted in the dashed circle. Inset: detailed footprint view near the tower. Sentinel images are from Copernicus Sentinel data 2024. c) Panoramic view of the setup, showing the eddy covariance mast (blue arrow/dashed box) and PTR-TOF-MS cabin (orange arrow/ dashed box).

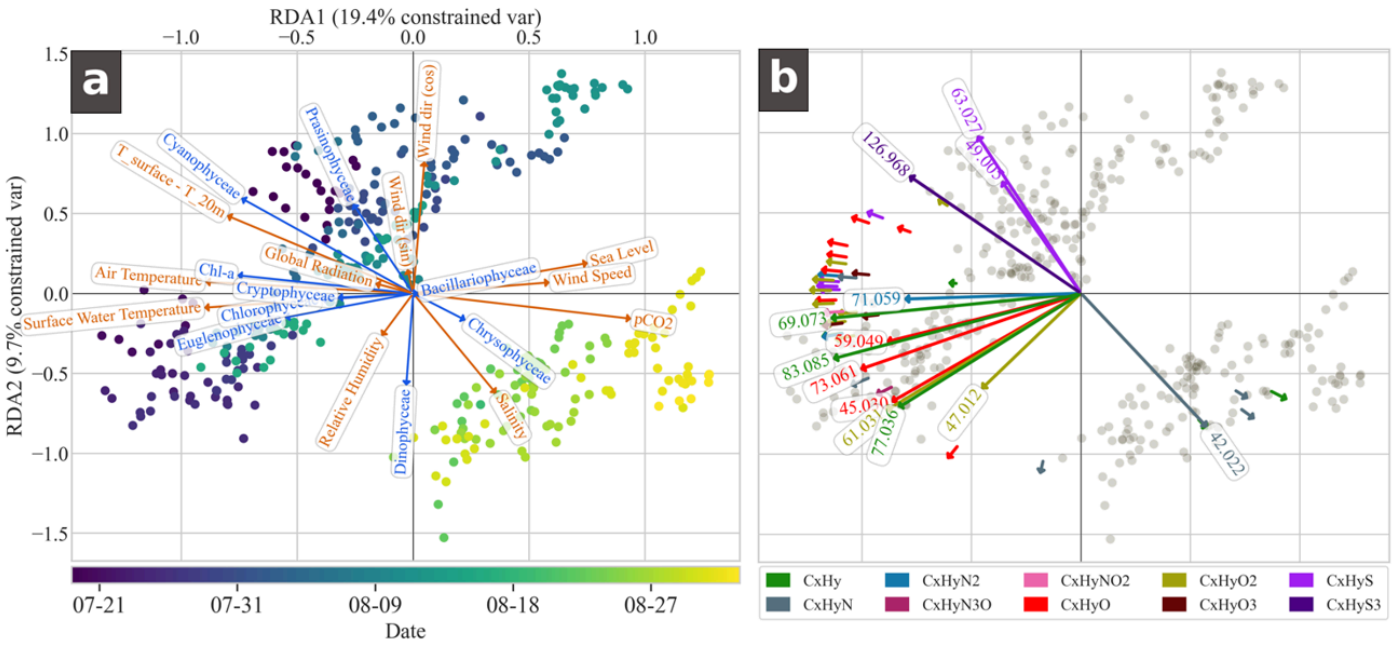


Figure 2

RDA of atmospheric VOC mixing ratios and environmental drivers. a) 1-h average scores (circles) colored by date. Vector length reflects explanatory strength (blue: biotic; orange: abiotic). The global constrained variance explained is R^2=0.79 (permutation p=0.001). b) m/z feature vectors colored by chemical groups; length indicates correlation strength. Most VOCs are shown as arrow tips, while dominant flux contributors (see Fig. 3a) are labeled vectors.

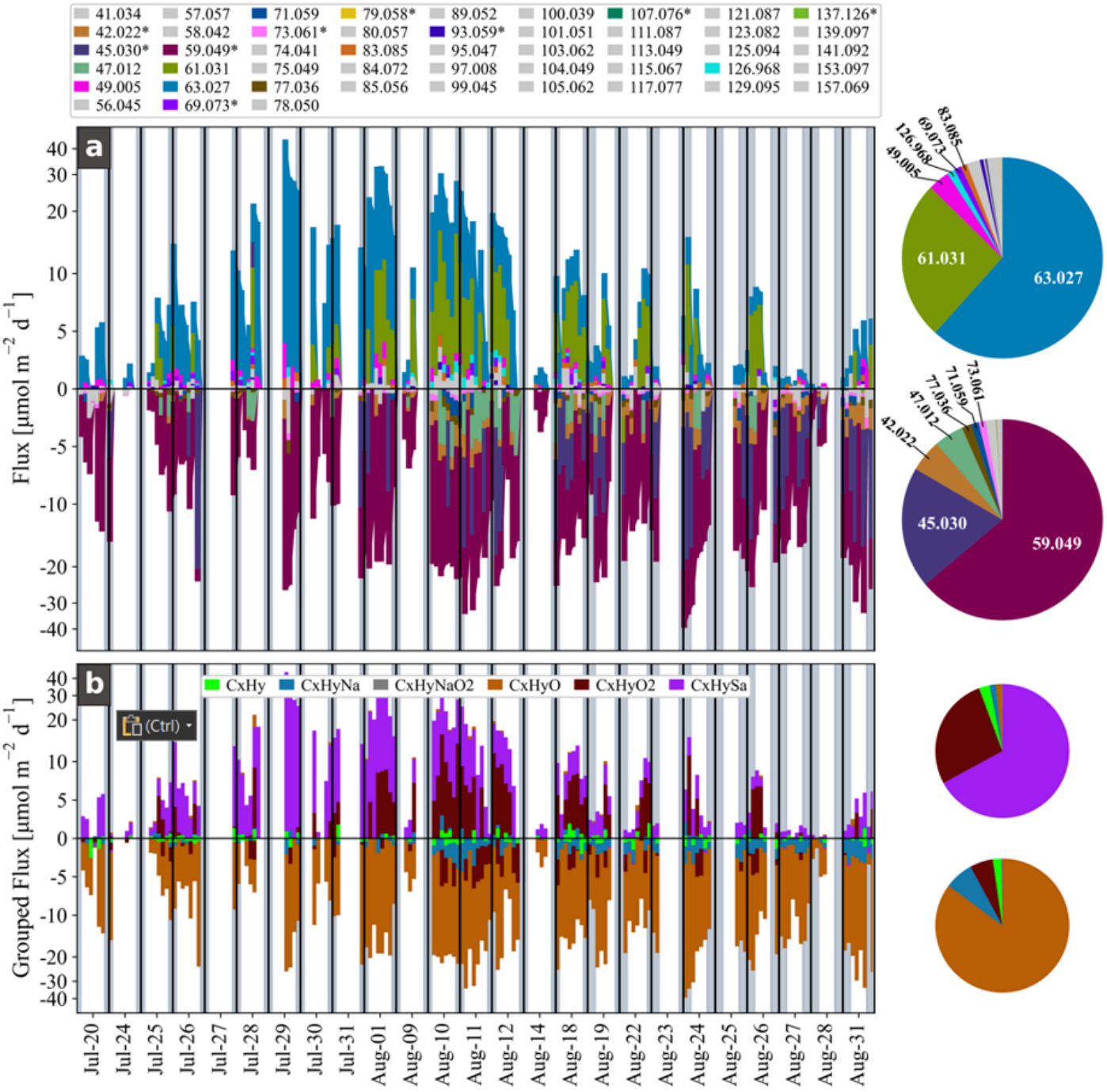


Figure 3

Three-hourly fluxes for filtered m/z features from marine footprint intervals; days without valid fluxes omitted. Y-axis uses combined linear (−10 to 10) and logarithmic (|flux| > 10) scales. Pie charts show campaign-averaged emission (top) and uptake (bottom) contributions by compound/group. Dark shadings indicate nighttime. a) Compound-resolved fluxes. Positive fluxes denote sea-to-air emission. Colors indicate individual features; "" denotes calibrated compounds. Small uncalibrated fluxes shown in gray. b) Fluxes summed by chemical groups.*

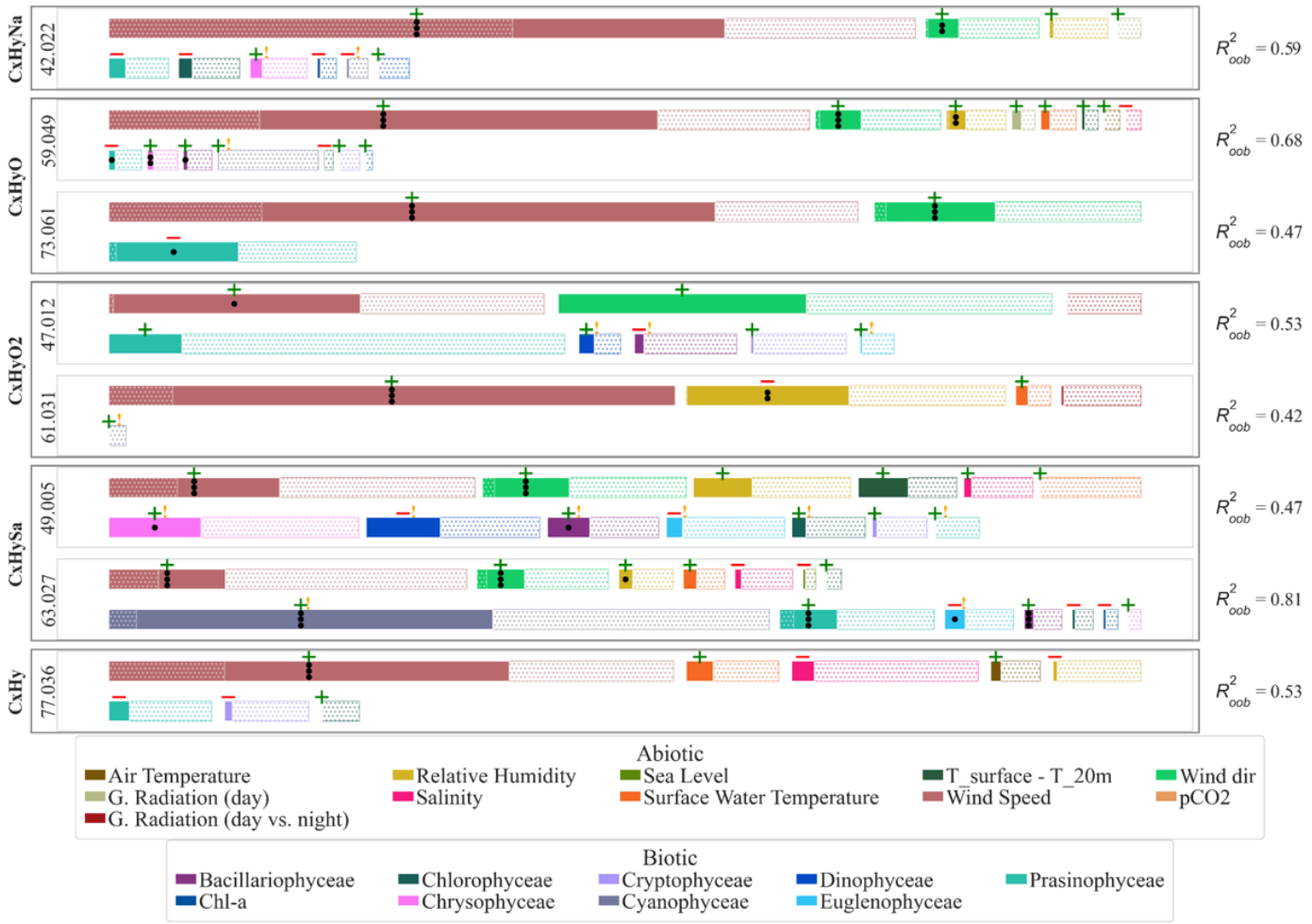


Figure 4

Predictor importance for VOC flux models. Bars show mean R² decrease after conditional permutation (n=100 repeats) with 95% bootstrap confidence intervals (dotted hatching). Significance: • p < 0.05, •• p < 0.01, ••• p < 0.001. Symbols indicate effect direction from partial dependence: + increasing, − decreasing, ! non-linear. Frames group compounds by chemical class. R^2_{oob} values (right) show out-of-bag performance. Conditional permutation used k=10 feature-space clusters.

Supplementary Files

This is a list of supplementary files associated with this preprint. Click to download.

- supplementaryinformation.pdf